Applied Energy 376 (2024) 124259

Contents lists available at ScienceDirect

Applied Energy

journal homepage: www.elsevier.com/locate/apenergy

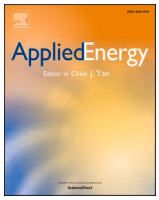

Operation optimization in large-scale heat pump systems: A scheduling framework integrating digital twin modelling, demand forecasting, and MILP

José Joaquín Aguilera [a,*], Roger Padullés [a], Wiebke Meesenburg [a], Wiebke Brix Markussen [b], Benjamin Zühlsdorf [b], Brian Elmegaard [a]

[a] Section of Thermal Energy, Department of Civil and Mechanical Engineering, Technical University of Denmark, Nils Koppels Alle 403, Kgs. Lyngby, 2800, Denmark
[b] Danish Technological Institute, Kongsvang Allé 29, Aarhus C, 8000, Denmark

HIGHLIGHTS

- Operation scheduling framework using MILP optimization and demand forecasting.
- Heat pump performance degradation due to fouling addressed through digital twins.
- Framework tested on a commercial system with heat pumps, TES and cooling towers.
- Up to 5% cost savings depending on forecasting accuracy and fouling levels.
- Savings from enhanced TES use and fouling-driven adjustment of heat pump operation.

ARTICLE INFO

Keywords:
Heat pump
Thermal energy storage
Operation scheduling
Digital twin
Fouling

ABSTRACT

The integration of large-scale heat pumps and thermal energy storage can facilitate sector coupling, potentially lowering heating and cooling costs in industries and buildings. This cost reduction can be extended by optimizing the utilization of the available thermal energy storage capacity in accordance to fluctuating electricity prices. Although the literature offers methods for optimizing the operation of these integrated systems, they often overlook the impact of heat pump performance degradation over time, such as from fouling. This oversight can lead to suboptimal system performance and inaccurate operational cost estimates. The present study addresses this gap by introducing a novel operational scheduling framework that aimed to reduce the operational costs of a commercial large-scale heat pump system. The system comprised an open cooling tower, a thermal storage tank and two heat pumps affected by fouling. The framework incorporated a mixed-integer linear programming (MILP) model, thermal demand forecasting, and heat pump performance maps that account for varying fouling levels. These maps were obtained from online calibrated simulation models used as digital twins of the heat pumps. The results demonstrated that the proposed framework enhanced the thermal energy storage utilization in response to variable electricity prices and adjusted the heat pump operation based on the influence of fouling. This resulted in a reduction of operational costs of up to 5% compared to the conventional operation of the system. These savings were observed to vary depending on the forecasting accuracy and the prevailing fouling levels. Overall, this study demonstrates the potential of using the proposed framework for cost reduction in large-scale heat pump systems.

1. Introduction

Current energy systems need to transition away from fossil fuels to meet the international treaty to minimize human impact on climate change [1]. Increasing the supply of low-to-zero-carbon electricity sources for heat production can reduce greenhouse gas emissions from the industrial and building energy sectors [2]. In the European Union (EU), fossil fuels make up 78% of the industrial process heat production, with electricity contributing only 3% [3]. In terms of the energy

* Corresponding author.
E-mail address: jojap@dtu.dk (J.J. Aguilera).

https://doi.org/10.1016/j.apenergy.2024.124259
Received 20 May 2024; Received in revised form 15 August 2024; Accepted 16 August 2024
Available online 24 August 2024

Nomenclature

Abbreviations

ACF	autocorrelation function
API	application programming interface
ARX	autoregressive model with exogenous inputs
BAU	business-as-usual
CF	correction factor
CIP	cleaning-in-place
CM	constant method
COP	coefficient of performance
CT	open cooling tower
err	error of the ARX
EU	European Union
FMU	functional mock-up unit
HP	heat pump
HPS	heat pump system
HS	high-stage
LM	linear method
LS	low-stage
MILP	mixed-integer linear programing
(N)RMSE	(normalized) root mean square error
SCADA	supervisory control and data acquisition
TES	thermal energy storage

Roman symbols

A	heat transfer area, m^2
b	constant, –
C	cost, €
E	thermal energy, MWh
K	forecast horizon, h
N	time interval, h
P	pressure, bar
Q	heat flow rate, kW
R	thermal resistance, K/kW
T	temperature, °C
U	overall heat transfer coefficient, kW/m^2K
u	binary variable, –
V	volume, m^3
V	volume flow rate, m^3/s
$\dot{W}$	power intake, MW
X	exogenous input, –
Y	forecasted thermal load, MW

Subscripts and superscripts

amb	ambient
clean	clean
c	cooling
cap	capacity
con	condenser
dem	demand
DSH	desuperheater
meas	measurement
e	evaporation
el	electricity
eva	evaporator
f	fouling
h	heating
in	inlet
op	operational
out	outlet
p	order of autoregressive model
s	discrete element
SC	sub-cooler
sim	simulation
sink	sink stream
source	source stream
t	time step
total	total
th	thermal
w	water

Greek symbols

β	calibration parameter, –
Δ	change, –
η	efficiency, –
θ	exogenous input coefficient, –
ρ	density, kg/m^3
Φ	autoregressive coefficient, –

produced for heating residential buildings in the EU, fossil fuels correspond to 57%, whereas electricity corresponds to 8% [4].

Large-scale electricity-driven heat pumps are among the most effective power-to-heat technologies that enable cross-sector integration [5]. Heat pumps can recover excess heat and leverage renewable energy sources for simultaneous heating and cooling applications such as industrial processes and district heating. Moreover, heat pumps have a higher heat output per electric energy input than conventional heating technologies such as gas boilers and electric heaters [6]. Yet, widespread adoption of heat pumps as a substitute for other heating technologies is limited due to risks related to elevated electricity prices and capital costs [7]. In this context, decreasing the operational costs of heat pumps is key for increasing the cost-effectiveness of this technology.

A key operational challenge heat pumps face are faults related to the heat sources they utilize. In large-scale heat pumps, one of the most common faults is the build-up of unwanted material deposition on the heat transfer surface of the source heat exchanger [8]. This deposition process, known as fouling, can be mitigated by non-invasive cleaning procedures such as cleaning-in-place (CIP) techniques. However, Pogiatzis et al. [9] highlighted that insufficiently planned fouling mitigation processes can accelerate the deterioration of heat exchangers and diminish the effectiveness of subsequent mitigation strategies.

Mixed integer linear programming (MILP) models are commonly used for techno-economic planning of energy systems, as indicated in [10]. MILP models enable to include a wide range of components, constraints and decision variables. The applicability of MILP models is limited to optimization problems that can be defined by linear mathematical expressions. For this reason, several studies that applied MILP for optimizing heat pump systems assumed a constant coefficient of performance (COP), such as in [11–14]. This neglects the nonlinear dependency of the COP on temperature and mass flow variations of the secondary streams of heat pumps. Verhelst et al. [15] defined a constant COP for the control of an air-to-water residential heat pump, which led to a higher electricity consumption compared to using more detailed COP estimates.

Several studies [16–18] proposed linear approximations of the COP from heat pumps. Recent studies included approximations of the COP in operation optimization and control frameworks for heat pump systems using MILP. Wirtz et al. [19] used a piecewise linearization of the COP dependency on the supply temperature from a district heating heat pump. Here, the COP was defined based on the corresponding supply temperature interval that was active. Krützfeldt et al. [20] proposed a design and operation optimization method for heat pump systems in residential buildings. In this approach, the relationship between the COP

of a heat pump and the temperatures of the secondary streams was represented by polynomial models, which were linearized via Taylor series. Maier et al. [21] compared linear, piecewise linear and quadratic approximations of the COP for a MILP-based model predictive control framework for a heat pump supplying a non-residential building. They found that the quadratic approach led to lower operational costs and computational time than the piecewise linear approach, while both approaches provided a more accurate representation of the COP compared to the simplified linear model. Another model predictive control based on MILP was proposed by Lee et al. [22], where it was assumed a linear dependency of the heat output and power consumption of a heat pump on the compressor speed as well as the sink and source temperatures.

Heat pump operation optimization and control frameworks based on MILP are often applied under known thermal energy loads [19]– [24] or use forecasted weather data from external sources as inputs to physical or data-driven models of such loads [25,26]. Another approach used in [23,25,27,28] is the assumption that the thermal energy loads for a given period are the same as those from the previous period, also known as naïve forecasting. In a few studies [29,30], the MILP-based optimization of heat pump systems integrated forecasting models for the thermal energy loads. Bünning et al. [29] used artificial neural networks to forecast the heating demand of a building. This demand was either covered with a heat pump or a thermal storage tank, which were operated through a model predictive controller. Nielsen et al. [30] applied an autoregressive forecasting model for the prediction of the heat demand for district heating operational planning. Here, the operational costs of heat pumps and electric boilers were compared over a forecasted period of 36 h.

Existing literature on operation scheduling and control for heat pumps lacks consideration for time-dependent performance degradation due to e.g. aging of components or faults like fouling. One model-based approach to account for performance degradation is the use of simulation models capable of adjusting at least part of their structure based on measured data, also referred to as digital twins. Examples of digital twins used for heat pump and refrigeration systems are included in a number of experimental studies [31]– [33]. Klingebiel et al. [31] used a self-optimizing model to implement defrosting cycles in a residential air-source heat pump. Chen et al. [32] monitored the degradation of the desiccant sorption material inside an absorption chiller through a digital twin. The digital twin was also used to optimize the COP of the chiller. Zhang et al. [33] proposed a model predictive control integrated with a digital twin to adjust the operation of a heat pump in real-time.

Only a few studies were found in the literature where performance degradation was monitored in commercial heat pumps used in industrial and district heating applications [34,35]. No previous studies were found where the degradation of the COP due to fouling was included for optimizing the operation of heat pump systems.

1.1. Contributions of this work

The present study aims at mapping the potentials for reducing the operational cost of large-scale heat pump systems through an online operation scheduling framework using digital twin technology. This framework integrated thermal demand forecasting and applied a MILP model for the optimization of a commercial large-scale heat pump system. The nonlinear relation between the COP of the heat pumps and their thermal energy loads was represented through a novel performance map. Unlike previous studies, this performance map was derived from a dynamic simulation model that was calibrated online to account for the time-dependent impact that fouling had on the COP.

2. Methods

The scheduling optimization framework was developed and tested on the large-scale heat pump system shown in Fig. 1, referred to as HPS hereafter. This system is used for district heating supply in Copenhagen, Denmark. The supply and return temperatures in the ink stream of the HPS are approximately 68 °C and 53 °C, respectively. At the same time, the HPS supplies industrial cooling to a biochemical plant, where it is required that a water stream is cooled down from around 23 °C to 18 °C.

The HPS is comprised of two identical heat pumps connected in parallel, an open cooling tower and a water tank used as thermal energy storage (TES). Each heat pump is an off-the-shelf two-stage unit with a

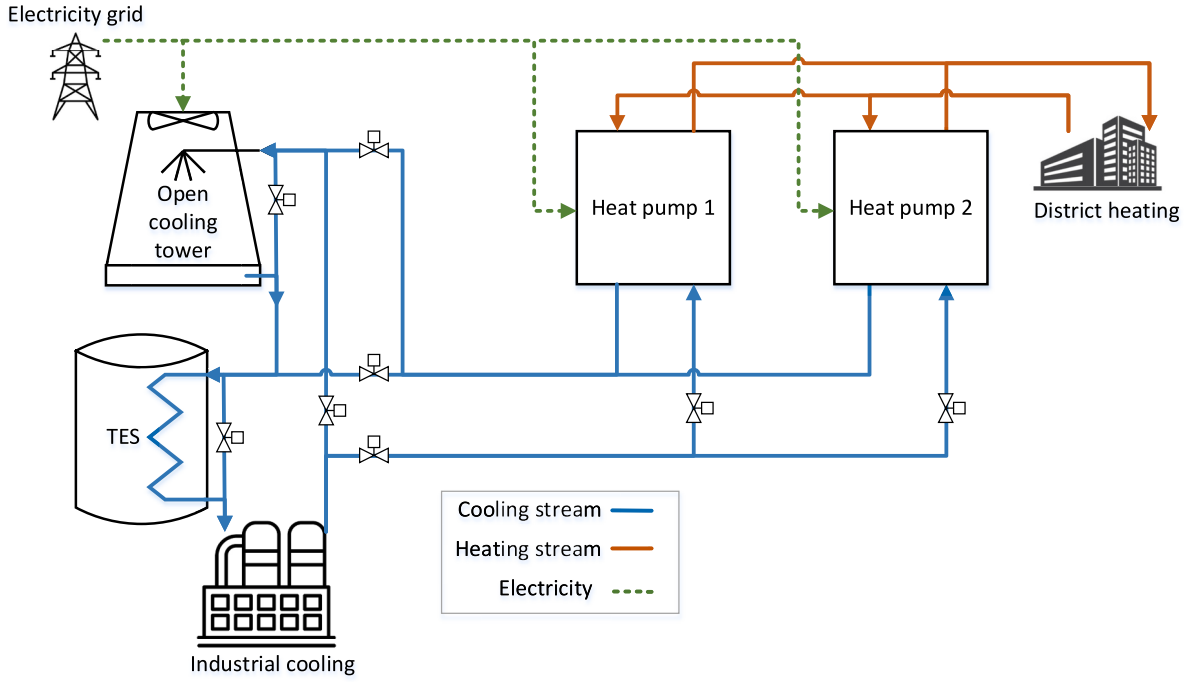

Fig. 1. Diagram of the components and streams in the HPS that were assessed in this study.

nominal heating capacity of 2 MW that uses ammonia as working fluid. The desuperheater, condenser, receiver and subcooler are included in a single shell-and-plate heat exchanger unit. The high and low stages are connected by an open intercooler. Each of the stages include a reciprocating compressor with a variable speed drive and an electronic expansion valve.

The evaporator is a shell-and-plate heat exchanger that is in direct contact with the water stream from the biochemical plant. This stream is contaminated with organic and inorganic substances that lead to fouling on the source side of the evaporator. Such substances result from the operation of the biochemical plant, and their exact chemical composition is unknown by the operator of the HPS and the authors of this study. It is not possible to open the evaporator for the removal of fouling. For this reason, a chemical cleaning-in-place (CIP) system is used, which does not require to dismantle the evaporator. This CIP process consists of the circulation of basic and acid solutions through the evaporator at different intervals for the removal of organic and inorganic substances, respectively. The frequency by which the CIP is used on each heat pump is determined heuristically by the HPS operator based on observations of the evaporation pressure.

The open cooling tower has a nominal cooling capacity of 8.3 MW and is comprised of 12 individual units. The fan in each unit has a nominal power consumption of 13 kW. The nominal flow rate as well as the inlet and outlet temperatures of the water in the cooling tower are 1351.1 m^3/h, 26.3 °C and 21 °C, respectively. The air wet bulb temperature and mass flow rate have design average values of 18 °C and 350 m^3/h, respectively.

The maximum and minimum temperatures of the water in the TES are 30 °C and 18 °C, respectively. The company owning the biochemical plant, which receives cooling from the HPS, did not reveal the specific volume of the TES. However, it was described that the purpose of the TES was to handle short variations in the water stream temperature to be cooled down caused by cleaning procedures of the equipment inside the plant. These variations occur as often as three to four times a day. In this context, it was assumed that the volume of the TES should not exceed the required cooling demand for six hours of HPS operation, which is equivalent to approximately 1000 m^3.

2.1. Business-as-usual operation

The current method to operate the HPS relies on a rule-based control strategy. The heat pumps operate unless undergoing maintenance. Their operation is dependent on the cooling demand, and the operation requirement from the district heating network aggregator. The TES is used as a cold storage. When the cold water stream at the outlet of the heat pumps exceeds the TES temperature, the TES stores heat. Conversely, if the cold water stream is below 18 °C, the TES is releases heat, which can be absorbed by the heat pumps or the cooling tower.

2.2. Online operation scheduling framework

The structure of the proposed framework for online operation scheduling of the HPS is shown in Fig. 2. The framework calculates a cost-effective schedule for operating the HPS as well as the costs and savings related to using this schedule compared to the business-as-usual operation of the system. This makes use of the existing infrastructure for storage and retrieval of operational data from the system, as well as weather data and electricity price data from publicly available sources.

The scheduling optimization is performed through a MILP model. Here, the operational cost of the HPS was minimized online by the use of a moving window approach. In this method, the optimization problem is solved repeatedly over consecutive time intervals, each with a fixed length of three days. The window, containing operational data, shifts through time, allowing for continuous adaptation and refinement of the operation schedule.

The heating and cooling demands driving the operation of the HPS were forecasted to determine an optimal operation schedule of the system in advance. This allows for the implementation of preventive measures rather than reactive responses during the operation of the HPS.

The COP of the heat pumps in the HPS under nominal and part-load operation were represented in the MILP model through a COP map. The COP map was derived from an off-design simulation model developed in the language Modelica [36]. The use of a simulation model enabled to represent the performance of the heat pumps under different thermal loads and fouling levels and compare to those present in the measured data retrieved from the HPS.

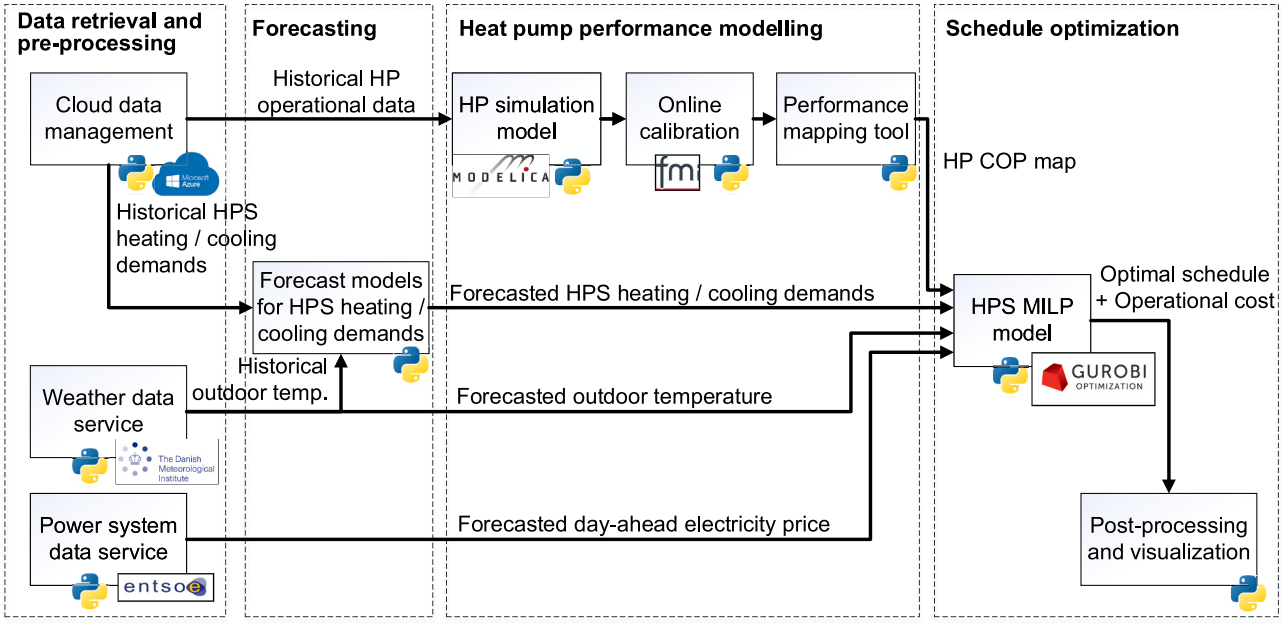

Fig. 2. Schematic of the proposed framework for operation scheduling.

2.3. Data retrieval and pre-processing

The data used in the proposed framework was retrieved remotely through Python from three different sources. These sources included a cloud data management system to collect operational data from the HPS as well as weather data and power system data services, which are available by means of application programmable interfaces (APIs).

Two five-day periods of HPS operation were used in the present study. These periods are referred to as period A and period B hereafter. As shown in Table 1, the cooling and heating demands from periods A and B were different, as well as the electricity prices. The mean heating demand shown in Table 1 was only related to the operation of the HPS and did not include the entire district heating network. Analysing the heating supplied by other technologies in the network, such as biomass boilers and combined heat and power plants, was beyond the scope of this study. The operation of the HPS was continuous during the operational periods A and B, which was a reason for their selection in the present study.

2.3.1. Cloud data management

The HPS is operated through a supervisory control and data acquisition (SCADA) system. The SCADA system was connected to the cloud computing service from Microsoft called Azure [37]. This enabled the remote access of operational data, which was comprised of data from sensing devices, actuators and control settings. This only included data from the two heat pumps and the cold and hot water streams in the HPS. Therefore, the operation of the open cooling tower and the TES was not monitored in real-time and only the design information from these components described in Section 2.1 was available.

The use of cloud computing technologies for remote monitoring and storage of operational data from industrial equipment has become increasingly popular in the last years, as mentioned in [38]. In the present study, it was only possible to retrieve data from the HPS to the API and not viceversa. The operational data from the HPS was collected at a one-minute interval and then converted into hourly average values.

2.3.2. Weather data and power system data services

The proposed framework applied the historical and predicted values of the outdoor air temperature (T_{amb}) and day-ahead electricity prices (c_{el}) in Copenhagen, Denmark. The value of T_{amb} was retrieved from the Danish Meteorological Institute through their Open Data API [39]. The day-ahead electricity prices were taken from the ENTSO-E API (European Network of Transmission System Operators for Electricity) [40]. These prices included a transmission grid tariff of 59 DKK/MWh and a system tariff of 24 DKK/MWh. The forecasting uncertainties of T_{amb} and c_{el} were neglected and the future values of these parameters were directly retrieved from [39,40], respectively. The data retrieved covered a three-day horizon.

2.4. Demand forecasting

The forecast horizon was three days and two days of historical operational data were used for the predictions. The forecasted heating or cooling demand over a horizon k was given in forecast of average values for every hour, which was represented by $Y_{t+k} = \{Q^{dem}_{t+1}, Q^{dem}_{t+2}, \ldots, Q^{dem}_{t+k}\}$.

Three forecasting methods were used with different complexity levels. The first method applied the mean value of the heating or cooling demands over a period n ($\bar{Y}_{t,n}$) as a constant forecasted value. This method was named CM (constant method) and is described by Eq. (1).

$$Y_{t+k} = \bar{Y}_{t,n} \tag{1}$$

The second forecasting method was referred to as LM (linear method), where a linear regression model was fitted between the historical heating and cooling demands and the outdoor air temperature. This model was used for predicting the future heating and cooling demands given forecasted values of the outdoor air temperature, as shown in Eq. (2).

$$Y_{t+k} = a_0 + a_1 \bullet X_{t+k} + e_{t+k} \tag{2}$$

where a_0 and a_1 are the regression coefficients obtained over a period n, $X_{t+k} = \{T_{amb,t+1}, T_{amb,t+2}, \ldots, T_{amb,t+k}\}$ is the time-series of outdoor air temperatures for the forecast horizon k, and e_{t+k} is the forecasting error.

The third forecasting method applied an autoregressive model with exogenous inputs, known as ARX. As described by Madsen [41], the AR part of the model uses lagged (or prior) states of the variable to forecast, whereas the exogenous input (i.e. the X term) represents a variable that is known in the future. In this study, the variable to forecast was either the heating or cooling demand. The exogenous input was the outdoor air temperature. This was included as historical and forecasted time-series data in the model and their retrieval was described in Section 2.3.2. The general formulation of an ARX model of order p is shown in Eq. (3). The value p defines how many prior states are used for forecasting.

$$\begin{aligned} Y_{t+k} = {} & b + \Phi_1 \bullet Y_{t-1} + \Phi_2 \bullet Y_{t-2} + \ldots + \Phi_p \bullet Y_{t-p} + \theta_1 \bullet X_{t-1} + \theta_2 \\ & \bullet X_{t-2} + \ldots + \theta_p \bullet X_{t-p} + e_{t+k} \end{aligned} \tag{3}$$

where b is a constant, Y_{t-1}, $Y_{t-2}\ldots Y_{t-p}$ are the lagged values of the heating or cooling demand, Φ_1, $\Phi_2\ldots \Phi_p$ are the autoregressive coefficients, θ_1, θ_2, …, θ_p are the coefficients for the outdoor air temperatures, e_{t+k} is the error of the model, and X_{t-1}, $X_{t-2}\ldots X_{t-p}$ are the lagged values of outdoor air temperatures.

The order of the ARX (p) is given by the time dependency of Y_t on its lag values. This was analyzed through the autocorrelation function (ACF) of the heating and cooling demands, shown in Fig. 3 a) and b), respectively. Both the ACF and ARX model were implemented in Python through the module statsmodels [42].

Fig. 3 a) shows that, after the first lags, the highest values of the ACF for the heating demand were found at approximately lags = 12 and 24. In this case, the order of the ARX was defined as $p = 12$. The order for the ARX for forecasting the cooling demand was defined as $p = 6$, given the time dependency of the ACF for this parameter, shown in Fig. 3 b).

The root mean square error (RMSE) and the normalized root mean square error (NRMSE) were used as evaluation measures for the performance of the forecasting methods. These errors were calculated based on measured (Y_t) and simulated values ($\hat{Y}_t$) of the heating and cooling demands, as shown in Eq. (4) and Eq. (5).

$$RMSE_k = \left(\frac{1}{k} \sum_{t=1}^{k} (Y_t - \hat{Y}_t)^2 \right)^{0.5} \tag{4}$$

Table 1
Summary of the main characteristics of the two operational periods analyzed.

Operational period	Start date	End date	Mean heating demand, MWh/day	Mean cooling demand, MWh/day	Mean hourly day-ahead electricity price, €/MWh	Mean hourly outdoor air temperature, °C
A	August 13, 2022	August 18, 2022	75.1	62.9	484.0	22.9
B	October 29, 2022	November 4, 2022	79.9	65.7	93.4	12.6

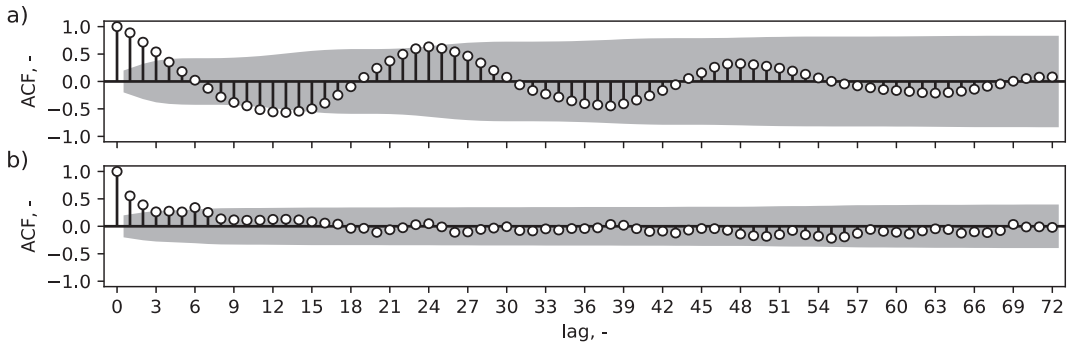

Fig. 3. Example of the autocorrelation function (ACF) of the heating demand a) and cooling demand b) for period B.

$$NRMSE_k = \frac{RMSE_k}{\overline{Y}_k} \quad (5)$$

The results of the scheduling optimization framework with and without the use of forecasting were compared with the business-as-usual operation of the HPS. This enabled the possibility to separate the uncertainties related to the forecasted heating and cooling demands. In this context, the framework without forecasting led to an optimized schedule of the HPS assuming that the heating and cooling demands were known.

2.5. Heat pump performance modelling

This section describes the use of a heat pump simulation model calibrated online for the development of the COP maps used for operation scheduling.

2.5.1. Heat pump simulation model

The heat pump simulation model, developed in Modelica, was implemented through the software Dymola [43] and the library TIL Suite [44]. This model is described in detail in a previous study [34]. This model was converted into a functional mockup unit (FMU) and simulated in Python by means of the FMPy module [45]. The inputs for the model included the volumetric flow rates of the source and sink streams ($\dot{V}_{source}$ and $\dot{V}_{sink}$, respectively), the inlet temperatures from the source and sink streams ($T_{source,in}$ and $T_{sink,in}$, respectively), along with the set points for intermediate pressure and source outlet temperature.

2.5.2. Online model calibration

The simulation model was adjusted based on measured data through two calibration processes: initial calibration and fouling calibration. A detailed description of the calibration processes is presented in [34]. In the initial calibration, the adjusted parameters were correction factors for the heat transfer coefficients in the desuperheater, condenser, subcooler and evaporator (CF_{DSH}, CF_{con}, CF_{SC} and CF_{eva}, respectively), as well as the integral time constants in the PI-controllers for the high-stage and low-stage compressors ($\tau_{com,HS}$ and $\tau_{com,LS}$, respectively). The initial calibration used operational data from the site acceptance test period. These data were available only from one heat pump, where its operation was adjusted under controlled conditions without the influence of fouling. Therefore, the results from the simulation model adjusted through the initial calibration were the same for both heat pumps in the HPS.

The fouling calibration relied on operational data obtained online from each heat pump. Here, the parameter adjusted was the thermal resistance related to fouling in the evaporator ($R_{th,f}$). This study focused only on fouling effects on the source side of the evaporator, as it was identified as a challenge by the HPS operator and had available measurements (e.g., evaporation pressure) to characterize fouling. There was insufficient information and measurements to analyze fouling effects on other components.

In this study, the periods chosen for fouling calibration were the last day of operation in periods A and B, described in Table 1. The final operational day was selected arbitrarily to serve as a representative example for the entire operational period. This choice was made in order to minimize the computational requirements during the fouling calibration process.

The optimization used for the calibration processes was performed through the Python module AixCaliBuHA [46] and applied the Powell optimization method available in the module SciPy [47]. The goal of the calibration processes was to minimize the normalized root mean square error between measured and simulated outputs, named calibration targets (γ), over a period 'n'. This minimization was performed iteratively to identify the value of the selected calibration parameters (β) that minimized the objective function shown in Eq. (6). The normalization was based on the mean of the measured calibration target over the period 'n' ($\overline{\gamma}$). The relevance of a target in the calibration processes was represented with a weighting factor (w). For the initial calibration, the targets included $\dot{Q}_{sink}$, the total power intake from both compressors ($\dot{W}_{com}$), and the evaporation pressure (p_e) with equal weight. In the fouling calibration, the only target was p_e.

$$minf(\beta) = \sum_{i=1}^{n} \left(w_i \bullet \overline{\gamma}_{meas}{}^{-1} \bullet \sqrt{n^{-1} \bullet \sum_{i=1}^{n} \left(\gamma_{sim,i}(\beta) - \gamma_{meas,i}\right)^2} \right) \quad (6)$$

2.5.3. Performance mapping tool

The calibrated simulation model was applied to develop a COP map of each heat pump. This map described the COP as a function of the load of a heat pump for a specific period of operation. A COP map enabled the calculation of the heat pump performance at different heat loads in the MILP model without the direct use of the simulation model. The different heat loads were obtained by varying the volume flow rate in the sink and source streams used as inputs to the model from their corresponding nominal values to 30% of those values. The variability of $\dot{V}_{sink}$ and $\dot{V}_{source}$ during those operational periods was much larger than that for $T_{sink,in}$ and $T_{source,in}$. This variability was described by the index of dispersion, namely the division between the variance of each time-dependent parameter over its mean value, shown in Table 2.

The relation between the simulated COP over different heat loads was represented by a quadratic regression model, which was then discretized. In this discretization, the heat load of the COP map was divided into equal intervals. The COP of each discrete interval was defined to be constant, maintaining a linear relationship between the heat capacity

Table 2
Index of dispersion for the measured input variables for the simulation model.

Operational period	Heat pump	$T_{source,in}$	$T_{sink,in}$	$\dot{V}_{sink}$	$\dot{V}_{source}$
A	1	0.02	0.01	0.68	0.36
	2	0.02	0.01	0.59	0.43
B	1	0.01	0.05	8.03	2.68
	2	0.01	0.05	8.08	3.90

and the power intake related to each interval, described in Section 2.6.3.

2.6. Schedule optimization

This section includes a description of the MILP used for optimizing the operational schedule of the HPS. Here, the variables of the model are presented with **bold** symbols. The MILP was solved using a time-step of 1-h and the selected solver was Gurobi [48].

The MILP model included the main components of the HPS system, namely the two heat pumps, the open cooling tower, the TES as well as the dynamic heating and cooling demands. The hydraulic pumps in the HPS were neglected. This was due to their low impact on the total power consumption.

2.6.1. Objective function

The objective function of the MILP model was the minimization of the total operational cost of the HPS $\mathbf{C}_{op}$ over a period k. As shown in Eq. (7), $\mathbf{C}_{op}$ was comprised of the electricity consumption from the heat pumps $\dot{\boldsymbol{W}}_t^{HP1}$ and $\dot{\boldsymbol{W}}_t^{HP2}$, as well as the electricity consumption from the fans in the open cooling tower $\dot{\boldsymbol{W}}_t^{CT}$. These variables were multiplied by the electricity price $c_{el,t}$ for every hour t of operation.

$$min(\mathbf{C}_{op}) = min\left(\sum_{t=1}^{k}\left(\dot{\boldsymbol{W}}_t^{HP1} + \dot{\boldsymbol{W}}_t^{HP2} + \dot{\boldsymbol{W}}_t^{CT}\right) \bullet c_{el,t}\right) \tag{7}$$

2.6.2. System level constraints

Eq. (8) and Eq. (9) show the thermal energy balances on the heating side and the cooling side of the HPS, respectively. Here, the heating demand $\dot{\boldsymbol{Q}}_t^{dem,h}$ needed to be covered in each period t by the heat flow rejected from any of the heat pumps, i.e. $\dot{\boldsymbol{Q}}_t^{HP1}$ and/or $\dot{\boldsymbol{Q}}_t^{HP2}$. The cooling demand was the sum of the heat flow to the evaporator of the heat pumps, the heat flow dissipated in the cooling tower $\dot{\boldsymbol{Q}}_t^{CT}$ and the heat flow to the TES $\dot{\boldsymbol{Q}}_t^{TES}$.

$$\dot{\boldsymbol{Q}}_t^{dem,h} = \dot{\boldsymbol{Q}}_t^{HP1,h} + \dot{\boldsymbol{Q}}_t^{HP2,h}, \forall t \in \{1,\ldots,k\} \tag{8}$$

$$\dot{\boldsymbol{Q}}_t^{dem,c} = \dot{\boldsymbol{Q}}_t^{HP1,c} + \dot{\boldsymbol{Q}}_t^{HP2,c} + \dot{\boldsymbol{Q}}_t^{CT} + \dot{\boldsymbol{Q}}_t^{TES}, \forall t \in \{1,\ldots,k\} \tag{9}$$

2.6.3. Heat pumps

The relationship between the heat output delivered by a heat pump and its power intake was determined by the COP map of that heat pump. This map was discretized according to the formulation presented in Appendix A. Fig. 4 exemplifies how the COP for a given capacity of a heat pump was determined through a COP map with four discrete elements. In this case, the heating delivered by heat pump 1 ($\dot{\boldsymbol{Q}}_t^{HP1,h}$) was above the capacity of the first segment ($\dot{\boldsymbol{Q}}_{s1}^{HP1,h,cap}$) and below that of the second segment ($\dot{\boldsymbol{Q}}_{s2}^{HP1,h,cap}$). Therefore, the resulting COP corresponded to that of the second segment (COP_{s2}^{HP1}). An increase in the number of discrete elements in a COP map will reduce the COP estimation error, shown in Fig. 4.

2.6.4. Open cooling tower

The electricity consumed by the fans in the open cooling tower ($\dot{\boldsymbol{W}}_t^{CT}$) was equal to the heat flow dissipated in this component ($\dot{\boldsymbol{Q}}_t^{CT}$) multiplied by the ratio between its nominal power consumption and its nominal cooling capacity ($\eta^{CT,fan}$), as represented by Eq. (10). The value of $\eta^{CT,fan}$ was assumed to be 2%, which was taken from the design characteristics of the cooling tower included in Section 2.1. $\dot{\boldsymbol{Q}}_t^{CT}$ was assumed to be unconstrained and thereby represented the cooling demand that was neither covered by the heat pumps nor by the TES.

$$\dot{\boldsymbol{W}}_t^{CT} = \dot{\boldsymbol{Q}}_t^{CT} \bullet \eta^{CT,fan}, \forall t \in \{1,\ldots,k\} \tag{10}$$

2.6.5. Thermal energy storage, TES

The sensible thermal storage capacity of the TES ($E^{TES,cap}$) was calculated based on Eq. (11). This capacity depended on the difference between the maximum and minimum temperature of the TES $T^{TES,max}$-$T^{TES,min}$, its volume V^{TES} as well as the water density ρ^{water} and specific heat c_p^{water}. The values of $T^{TES,max}$ and $T^{TES,min}$ were 30 °C and 18 °C, respectively; V^{TES} was 200 m^3 and was varied up to 1000 m^3 within a sensitivity analysis; whereas ρ^{water} and c_p^{water} were 998 kg/m^3 and 4.18 kJ/kg•K, respectively.

$$E^{TES,cap} = V^{TES} \bullet \rho^{water} \bullet c_p^{water} \bullet \left(T^{TES,max} - T^{TES,min}\right) \tag{11}$$

Eq. (12) was applied to determine the stored thermal energy in the TES $\boldsymbol{E}_t^{TES}$ at any time-step t. This depended on the energy stored in the previous time-step $\boldsymbol{E}_{t-1}^{TES}$ and the heat flow to and from the TES, denoted by a positive or negative value of $\dot{\boldsymbol{Q}}_t^{TES}$, respectively. Given that the temperatures of the TES were equal or below 30 °C, it was assumed that its heat losses to the environment were negligible. Moreover, it was assumed that at the start and end of the evaluation period (i.e. $t = 1$ and $t = k$) the thermal energy stored in the TES was equal to half of its total capacity.

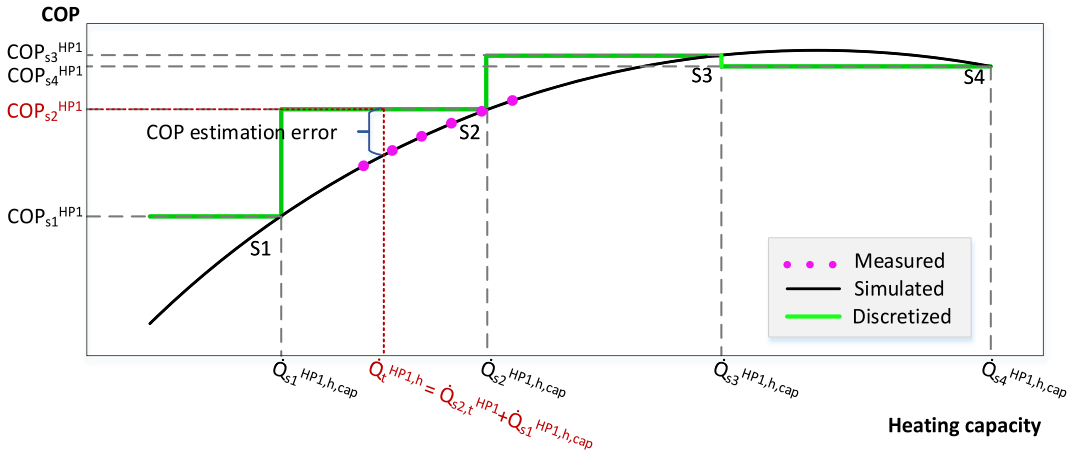

Fig. 4. Example of the discretized COP map of heat pump 1 with four discrete elements. The heating capacity delivered by the heat pump and its corresponding COP are shown in red. (For interpretation of the references to colour in this figure legend, the reader is referred to the web version of this article.)

$$\boldsymbol{E}_t^{\mathrm{TES}} = \begin{cases} 0.5 \bullet E^{\mathrm{TES,cap}} \text{ if } t = 1 \\ \boldsymbol{E}_{t-1}^{\mathrm{TES}} - \dot{\boldsymbol{Q}}_{t-1}^{\mathrm{TES}} \bullet \Delta t \text{ if } 1 < t < k \\ 0.5 \bullet E^{\mathrm{TES,cap}} \text{ if } t = k \end{cases} \quad (12)$$

3. Results

3.1. Model calibration

The results from the calibration of the simulation model are presented in Table 3. This includes the results from the initial calibration performed once using the site test period data and the fouling calibration performed twice on each heat pump, were the operational data from periods A and B were applied. Among the correction factors adjusted in the initial calibration, the correction factor related to the evaporator heat transfer coefficient required the largest adjustment. The relatively large values obtained for the time-constants of the compressor controllers was attributed to the slow dynamics present in the HPS. The fouling calibration showed that the thermal resistance related to fouling was around 14% larger in heat pump 1 compared to heat pump 2 in period A. In period B, the fouling thermal resistance of heat pump 2 exceeded that of heat pump 1 by approximately 25%.

3.2. Heat pump performance mapping

Fig. 5 shows how the average computation time for solving the MILP optimization and the RMSE in estimating COP were affected by varying the number of discrete elements used to define COP maps of both heat pumps in the HPS. More discrete elements required a longer period to solve the optimization, which also decreased the RMSE related to the estimation of the COP. As seen in Fig. 5, using more than approximately 35 discrete elements did not show a reduction of the RMSE and increased the computation time. Based on this, the COP maps used in this study applied 35 discrete elements.

The COP maps for heat pumps in the HPS are shown in Fig. 6. These maps illustrate the performance of the heat pumps with and without the influence of the fouling-related thermal resistances during periods A and B (shown in Table 3). Additionally, the maps include the RMSE for the COP estimation, along with the average sink and source inlet temperatures for period A (50 °C /27 °C) and period B (49 °C /25 °C). The results showed that an increased level of fouling in a heat pump led to a reduction of its COP for a given normalized heat load, as shown in Fig. 6.

Table 3
Results from the initial model calibration and fouling calibration for both heat pumps in the HPS.

Calibration process	Operational period	Heat pump	Calibrated parameter	Value	NRMSE
Initial calibration	Site acceptance test	1 and 2	CF_{eva}	1.5	4.4%
			CF_{DSH}	1.2	1.6%
			CF_{con}	1.0	1.2%
			CF_{sub}	0.7	2.3%
			$Ti_{com,HS}$	1461.4 s	6.0%
			$Ti_{com,LS}$	1944.1 s	5.4%
Fouling calibration	A	1	$R_{th,f}$	$2.5 \bullet 10^{-3}$ K/kW	3.7%
		2	$R_{th,f}$	$2.2 \bullet 10^{-3}$ K/kW	2.2%
	B	1	$R_{th,f}$	$2.0 \bullet 10^{-3}$ K/kW	3.4%
		2	$R_{th,f}$	$2.5 \bullet 10^{-3}$ K/kW	4.1%

3.3. Forecasting

The forecasting methods presented in Section 2.4 were compared in terms of the errors obtained from the forecasted heating and cooling demands that drive the operation of the HPS. Fig. 7 shows a comparison between the forecasted heating and cooling demands for 3-day forecast horizons for the operational periods A and B. These results show that the forecasted heating demand from the ARX and the LM generally followed the heating demand, particularly on the first forecasted day. The forecasted cooling demands from the CM, LM and ARX were constant and with similar values. Period A contained sudden reductions of the heating and cooling loads which were not stationary and did not depend on the outdoor air temperature. These variations were not captured by any of the forecasting methods.

Table 4 displays the errors derived from the forecasting methods for the last three days of operation in periods A and B. The heating demand forecasts from the ARX method yielded NRMSE values between 0.1% and 0.5%-points lower than those obtained from the CM and LM methods. For the forecasted cooling demand, the ARX method consistently exhibited the lowest RMSE across most cases presented in Table 4. The variations in the cooling demand were neither stationary nor influenced by outdoor air temperature, contributing to the CM outperforming the LM and ARX.

3.4. Comparison between scenarios

Fig. 8 shows the total cooling provided by each component in the HPS over the last three days of operation in periods A and B. This includes the results from the BAU operation and from the optimization without forecasting and with forecasting using the ARX method. The schedule optimization led to an increase of the cooling provided by the TES compared to the BAU operation. This increase without forecasting was 1.7 and 0.4 percentage points for periods A and B, respectively. With forecasting, such increase reached 5.5 and 1.2 percentage points for periods A and B, respectively. The optimization also adjusted the operation of both heat pumps in the system based on the extent to which their performance was affected by fouling (seen in Fig. 6). As shown in Fig. 8, a larger fraction of the total cooling supplied was provided by the heat pump less affected by fouling, which in period A was heat pump 2 and in period B was heat pump 1.

The relation between the electricity prices and the operation of the HPS is shown in Fig. 9 and Fig. 10 for periods A and B, respectively. This includes the temperature of the TES, the normalized heat load of both heat pumps, along with the operational cost for the BAU operation and the schedule optimization without forecasting and with the ARX forecasting. Fig. 9 and Fig. 10 show that under the optimization cases, the temperature of the TES increased in periods where the electricity price increased and decreased in periods where the electricity price was reduced. In contrast to the BAU operation, the schedule optimization involved multiple cycles in which the temperature of the TES reached its minimum and maximum values over the three days of operation. This led to lower operational costs in the optimized operation of the HPS compared to its BAU operation. A larger cost reduction was achieved during period A, characterized by higher electricity prices compared to period B. Additionally, the BAU operation in period A exhibited less cooling provided by the TES and a larger fraction of the cooling supplied by the cooling tower compared to period B, as seen in Fig. 8. This contributed to a comparatively smaller reduction in operational costs when using the optimization on period B than on period A.

3.5. Influence of fouling and TES volume

Fig. 11 shows the total operational costs of the schedule optimization framework and its savings compared to the BAU case for periods A and B for TES volumes between 200 m^3 to 1000 m^3. Fig. 11 shows the relative change between the total operational costs related to a TES volume of

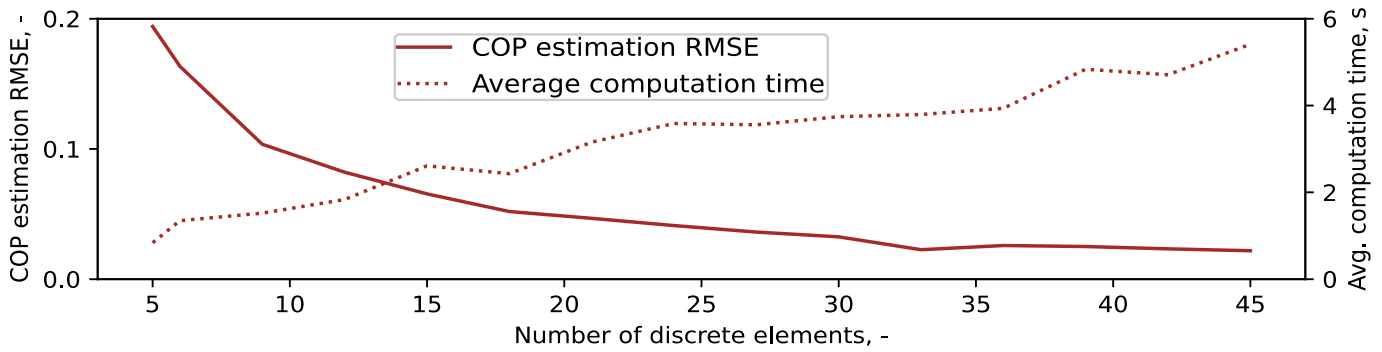

Fig. 5. Relation between the number of discrete elements and the RMSE derived from the COP map from both heat pumps as well as the average computation time related to solving the MILP optimization process.

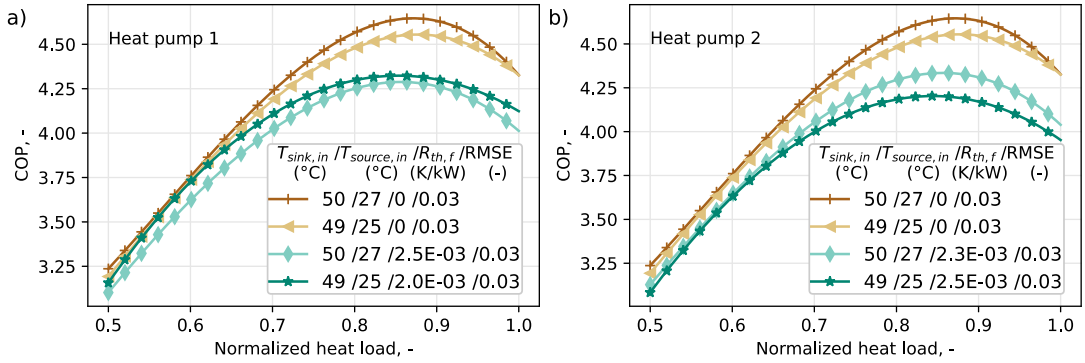

Fig. 6. COP map for heat pump 1 (a) and heat pump 2 (b). The figures were cut to show the range between the minimum normalized heat load used to build the maps (0.5) and its maximum value (1). The maps include the sink and source temperatures in each period, as well as the RMSE. $R_{th,f}$: evaporator thermal resistance attributed to fouling.

200 m^3 and operational costs linked to higher TES volumes, named relative cost difference. These results included the heat pumps affected by the fouling thermal resistance values presented in Table 3. As seen in Fig. 11, the savings related to the schedule optimization were greater in period A than in period B. These savings were around 5.2% when using forecasting and 3.4% without forecasting for period A, considering a TES volume of 200 m^3. For the same TES volume, the savings for period B were 1.6% and 0.7% with and without the use of forecasting, respectively. For any given case, the difference between savings using 200 m^3 and 1000 m^3 was lower than 0.2%.

The influence of the thermal resistance on the operational costs due to fouling and savings derived from the operation scheduling framework are shown in Fig. 12. Here, the fouling thermal resistance affecting both heat pumps in the HPS were assumed to be equal. The relative cost difference specifically represents the relative change between the total operational costs related to a zero fouling level and those connected with non-zero fouling levels. The results from Fig. 12 showed that not considering fouling caused an overestimation of the savings obtained when using the operation scheduling framework rather than BAU operation. An increase of the fouling thermal resistance above the levels observed in the present study (i.e. between $2•10^{-3}$ K/kW and $2.5•10^{-3}$ K/kW, as seen in Table 3) increased the operational costs. This increase was up to approximately 7% to 8% for a fouling thermal resistance of $4•10^{-3}$ K/kW. At that fouling level, the savings derived from the framework were reduced by approximately 2 percentage points compared to the case without the presence of fouling. This was caused by keeping the fouling thermal resistance constant in the business-as-usual operation and increasing it in the proposed framework.

4. Discussion

The replacement of the rule-based business-as-usual operation of the HPS with the proposed online operation scheduling framework was observed to reduce the operational costs of such a system up to 5.2% with forecasting and 3.4% without forecasting. The cost reduction was driven by two key factors. The first factor was leveraging the TES thermal storage capacity in response to varying electricity prices. The second factor was attributed to switching between the two heat pump units based on the impact of fouling on their performance. Both factors aimed to decrease the cooling demand supplied by the cooling tower, which was greater decreased in period A compared to period B (see Fig. 8). The first factor had a greater impact on cost savings than the second, as the difference in fouling-related thermal resistances between the heat pumps was larger in period B than in period A (see Table 3). However, it is not possible to derive conclusions on the relative importance of each factor on cost savings. This is because such a comparison depends on variations in boundary conditions such as fouling levels and thermal demands across different periods.

Optimizing the utilization of the thermal storage tank did not result in significant differences in operational costs, as shown in Fig. 11. In the HPS used as a case study, a significant portion of the cooling demand was met by the heat extracted from the heat pumps used for district heating supply. Due to the high heating demand during the analyzed periods, the heat pumps operated close to their nominal load. Hence, the influence of the optimization on operational costs, whether through thermal energy storage utilization or adjusting heat pump operation, was limited. However, the proposed framework may offer more significant cost savings in heat pump systems with less constrained operational conditions than those encountered in our present study.

The online scheduling framework in this study was developed based

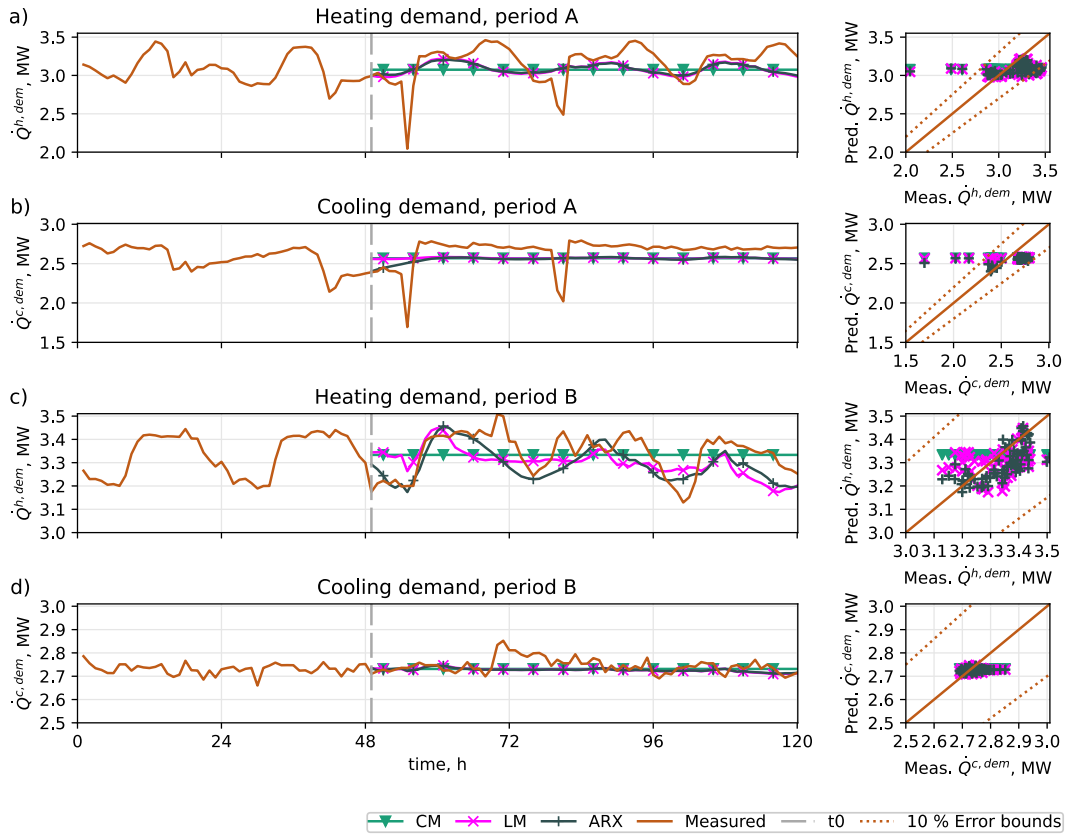

Fig. 7. Heating and cooling demands from periods A and B, where the last three days were forecasted by using CM, LM and ARX. The axes in the plots are not in scale to illustrate the differences between the results from the forecasting methods. Pred.: predicted; Meas.: measured.

Table 4
Errors obtained from the forecasting of the heating and cooling demands by using CM, LM and ARX.

Period	Forecasted parameter	CM	LM	ARX
		RMSE / NRMSE, kW / %		
A	Heating demand	256 / 8.0	240 / 7.6	240 / 7.5
	Cooling demand	197 / 7.4	195 / 7.3	190 / 7.2
B	Heating demand	87 / 2.6	97 / 2.9	69 / 2.1
	Cooling demand	35 / 1.3	37 / 1.4	37 / 1.3

on existing resources, namely the data from the SCADA system in the HPS, along with openly available information from weather and electricity market platforms. Additionally, a heat pump simulation model from a previous study [34] was employed. While this demonstrates the potential for reusing simulation models, it is important to note that the model used in this study was not specifically designed for an online optimization framework. As opposed to detailed simulation models, simpler models may be more appropriate for such tasks, requiring less assumptions for their development and less time for their simulation.

The difference between the simulation results from the two heat pumps in the HPS was only attributed to the fouling thermal resistance. Neglecting factors in the simulation model such as the presence of oil and non-condensables in the refrigerant side, non-nominal refrigerant

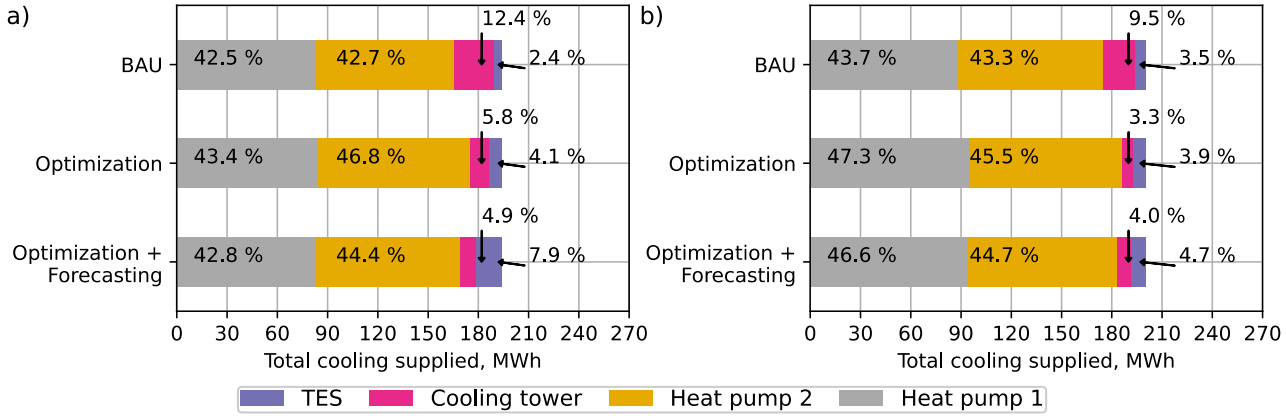

Fig. 8. Cooling supplied by the different components in the HPS when considering the BAU operation or the MILP optimization with and without forecasting. Periods A and B are shown in a) and b), respectively.

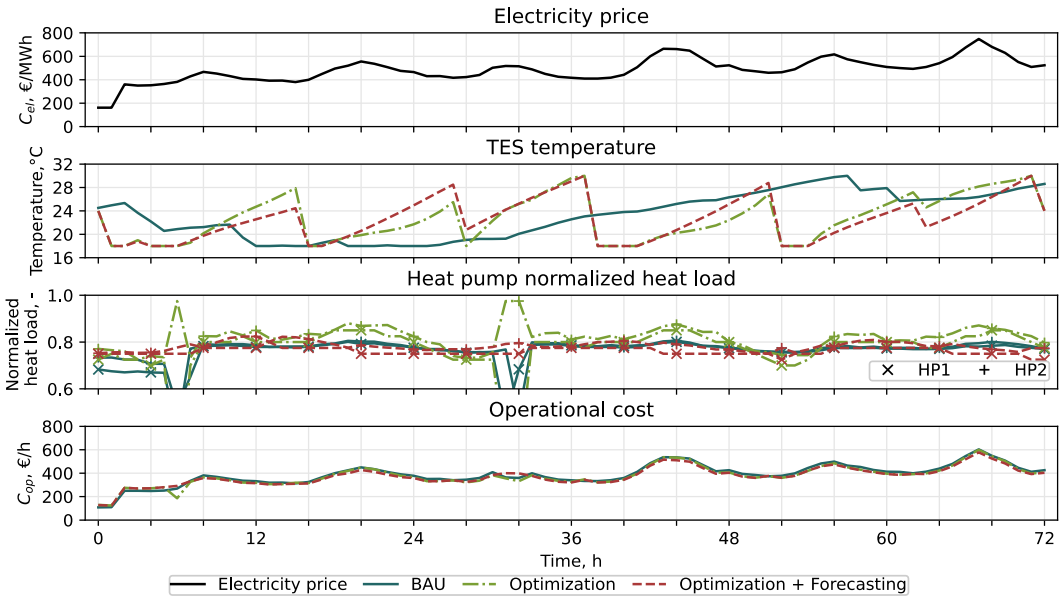

Fig. 9. BAU operation compared to the MILP optimization with and without forecasting for period A.

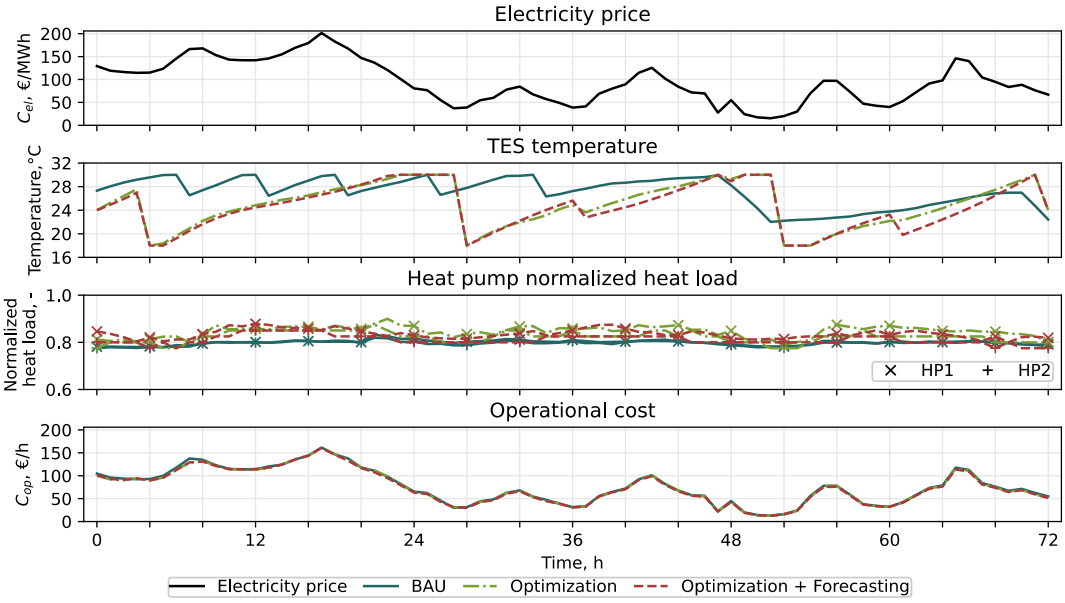

Fig. 10. BAU operation compared to the MILP optimization with and without forecasting for period B.

charge and heat losses in the components, led to discrepancies between simulated and measured values. The inclusion of these additional sources of discrepancy requires increasing the number of calibration parameters and targets in the online calibration. This would raise the number of assumptions needed (e.g. selection of weighting factors, calibration periods) and the computational requirements for the online calibration process.

The simplifications made regarding the operation of the TES and the open cooling tower likely influenced the results of this study. These simplifications included neglecting heat losses and thermal stratification in the TES, as well as the dependency of the cooling tower capacity on outdoor conditions and water inlet streams. Using more detailed models of the thermal storage tank, as done in several related studies [49–51], may lead to more accurate estimations of the system's operation costs than those presented in Section 3.4. However, the use of detailed models will also require longer computational times than the results shown in Fig. 5. Accounting for phenomena such as thermal stratification necessitates design information of the TES, which was not available from the HPS assessed in this study. This represents an opportunity to enhance the proposed framework in future studies.

The COP maps employed in this study are simple to generate, offering rapid estimates of heat pump performance and compatibility with MILP models. However, their accuracy may be limited when applied to diverse boundary conditions not covered in the operational periods assessed in this study. While changes in the volume flow rates of the secondary streams were assumed to have the largest effect on the COP (as observed in Table 2), other parameters could exert a greater influence on the COP during different operational periods. This may result in different COP maps structures (e.g. linear, quadratic), as noted by Pieper et al. [18].

The simulation and calibration steps in the proposed operation scheduling framework were related to modelling errors, which were

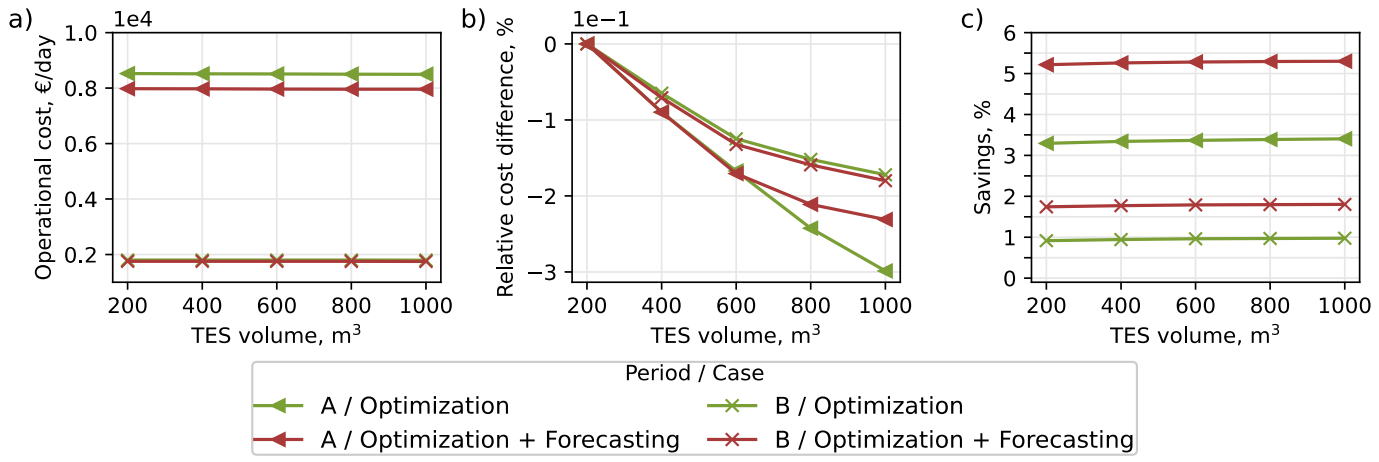

Fig. 11. Operational costs and savings when operating based on the schedule optimization instead of BAU operation, accounting for different TES volumes.

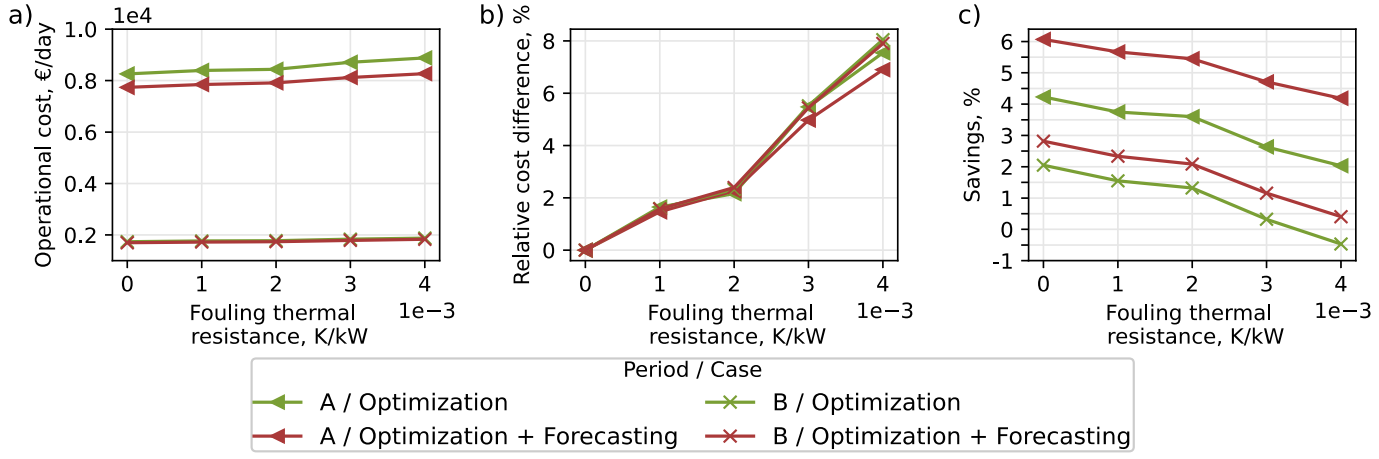

Fig. 12. Operational costs and savings when operating based on the schedule optimization instead of BAU operation, accounting for different fouling thermal resistances.

represented by the NRMSE values shown in Table 3. In this context, if an operational period under assessment (e.g. period A) enabled characterizing the COP over a wide range of loads (e.g. from 0.5 to 1), it would be preferred to use the operational data from that period directly to develop the COP maps rather than a simulation model. The use of a simulation model for developing the COP maps enabled to calculate the COP of the heat pumps at loads that were not observed from the measured data. This approach is particularly useful for commercial heat pumps like the HPS assessed in this study, where the operation of the heat pump cannot be modified to obtain a representative COP map from a given operational period.

When contrasting the MILP optimization results with and without forecasting, it was noted that the operational cost savings related to the online operation scheduling framework were overestimated when accounting for the forecasting errors (see Fig. 11 and Fig. 12). Larger forecasting errors than those described in this study (see Table 4) are expected for longer forecast horizons than three days and when accounting for the uncertainty of the forecasted electricity prices and outdoor air temperatures. In this context, it is unlikely that the proposed online operation scheduling framework will provide accurate results for forecast horizons beyond five days, where the uncertainty of weather forecasts tend to increase [52].

The ARX method provided more accurate predictions for heating demand compared to the constant and linear methods, although the NRMSE differences between all tested methods were only between 0.1% and 0.8%, as shown in Table 4. However, using operational data over longer periods than in this study would better highlight the differences between the methods used. The ARX outperformed the other methods due to its compatibility with the stationary nature of the heating demand and its dependence on the outdoor temperature. For this reason, previous studies [53–55] also used ARX for heating demand forecasting in buildings. Moreover, as seen in Section 2.4, the ARX was relatively simple to implement, but may require to be re-adjusted due to different seasonal patterns of the heating demand throughout a year or due to changes in heating and electricity prices. Regarding the forecasting of the cooling demand, no large differences were obtained across the forecasting methods assessed in this study.

The estimation of the current fouling thermal resistance (see Table 3) and the operational costs of the HPS under different fouling levels (see Fig. 12) could be applied for predictive maintenance. This involves providing a cost-effective plan that specifies the timing and which specific heat pump within the system the CIP should be applied to. Here, the results from the optimized and forecasted operation of the system from the proposed framework will need to be complemented with information about CIP costs, CIP effectiveness, and forecasted values of heating prices, cooling prices as well as fouling thermal resistance. Attempts of forecasting fouling for model-based predictive maintenance in large-scale heat pumps was done in an earlier study [56]. However, further research is needed in that direction since no studies were found in the literature where model-based predictive maintenance was continuously applied in operating large-scale heat pump systems.

5. Conclusions

The present study aimed at reducing the operational cost of a commercial large-scale heat pump system by using a digital twin-based framework for online operation optimization. The system supplied district heating as well as industrial cooling simultaneously and was comprised of two heat pumps, an open cooling tower and a thermal energy storage tank. Both heat pumps in the system were constantly affected by evaporator fouling. The proposed framework used a mixed-integer linear programming (MILP) model integrated with thermal demand forecasting and heat pump performance maps adjusted for different levels of fouling through a simulation model calibrated online. This model was adjusted through an initial calibration, where heat transfer coefficients and control dynamics in the model were adjusted, and a fouling calibration process, where the evaporator thermal resistance attributed to fouling was determined. Two periods of operation were assessed in this study, where the different levels of fouling were identified through the fouling calibration process. Three methods were compared for the forecasting of the heating and cooling demands, including a constant method, a linear method, and an autoregressive model with exogenous inputs. Compared to the business-as-usual operation of the system, the optimization increased utilization of the thermal energy storage by up to 5 percentage points as a result of variable electricity prices. The optimization also enabled the adjustment of the heat pump operation based on the influence of fouling. The optimized operation of the system resulted in operational cost savings up to 5% with forecasting and 3% without forecasting, compared to its conventional operation. A sensitivity analysis on the impact of fouling on operational costs highlighted the necessity of accurate fouling representation for reliable savings estimation in the proposed scheduling framework. Overall, the framework demonstrated potential for cost reduction in large-scale heat pump systems, with savings influenced by forecast accuracy and prevalent fouling levels.

CRediT authorship contribution statement

José Joaquín Aguilera: Writing – review & editing, Writing – original draft, Visualization, Validation, Software, Methodology, Investigation, Formal analysis, Data curation, Conceptualization. **Roger Padullés:** Writing – review & editing, Software, Methodology, Formal analysis, Conceptualization. **Wiebke Meesenburg:** Writing – review & editing, Validation, Supervision, Project administration, Methodology, Formal analysis. **Wiebke Brix Markussen:** Writing – review & editing, Validation, Supervision, Formal analysis, Conceptualization. **Benjamin Zühlsdorf:** Writing – review & editing, Supervision, Funding acquisition. **Brian Elmegaard:** Writing – review & editing, Validation, Supervision, Project administration, Funding acquisition.

Declaration of competing interest

The authors declare that they have no known competing financial interests or personal relationships that could have appeared to influence the work reported in this paper.

Data availability

The authors do not have permission to share data.

Acknowledgements

This work was funded by EUDP (Energy Technology Development and Demonstration) under the project “Digital twins for large-scale heat pump and refrigeration systems” (project number: 64019-0570).

Appendix A

This appendix provides a description of the discretization process applied to the COP maps from the heat pumps included in the MILP optimization. The energy balance of each heat pump was described by Eq. (13). Here, the heat flow from the condenser unit $\dot{Q}_t^{HP,h}$ and the heat flow to the evaporator $\dot{Q}_t^{HP,c}$ were the sum of the heat flows from all S discretization elements $\dot{Q}_{s,t}^{HP,h}$ and $\dot{Q}_{s,t}^{HP,c}$, (respectively)

$$\dot{W}_t^{HP} = \dot{Q}_t^{HP,h} - \dot{Q}_t^{HP,c}, \forall t \in \{1,\ldots,k\} \tag{13}$$

$$\dot{Q}_t^{HP,h} = \sum_{s=1}^{S}\left(\dot{Q}_{s,t}^{HP,h}\right), \forall t \in \{1,\ldots,k\} \tag{14}$$

$$\dot{Q}_t^{HP,c} = \sum_{s=1}^{S}\left(\dot{Q}_{s,t}^{HP,c}\right), \forall t \in \{1,\ldots,k\} \tag{15}$$

The heat flow to each discretization element $\dot{Q}_{s,t}^{HP,c}$ was constrained by the cooling capacity of the element $\dot{Q}_{s,t}^{HP,c,cap}$ multiplied by a binary variable $u_{s,t}^{HP}$, as shown in Eq. (16). This binary variable was equal to 1 if the element s was active and 0 otherwise.

$$\dot{Q}_{s,t}^{HP,c} \le \dot{Q}_s^{HP,c,cap} \bullet u_{s,t}^{HP}, \forall s \in \{1,\ldots,S\}, \forall t \in \{1,\ldots,k\} \tag{16}$$

Eq. (17) ensured that the relation between the heating supplied by all discretization elements until an element s (i.e. $\dot{Q}_s^{HP,h} + \dot{Q}_{s-1}^{HP,h,cap}$) and the cooling supplied by all discretization elements until an element s (i.e. $\dot{Q}_s^{HP,c} + \dot{Q}_{s-1}^{HP,c,cap}$) was defined in terms of the COP of this element COP_s^{HP}. The value of COP_s^{HP}, $\dot{Q}_s^{HP,c,cap}$ and $\dot{Q}_s^{HP,h,cap}$ for all discretization elements were obtained from the COP map described in Section 0.

$$\dot{Q}_{s,t}^{HP,h} = \begin{cases} \dot{Q}_{s,t}^{HP,c} \bullet \dfrac{COP_s^{HP}}{COP_s^{HP}-1}, \text{if } s = 1 \\ \left(\dot{Q}_{s,t}^{HP,c} + \dot{Q}_{s-1}^{HP,c,cap} \bullet u_{s,t}^{HP}\right) \bullet \dfrac{COP_s^{HP}}{COP_s^{HP}-1} - \dot{Q}_{s-1}^{HP,h,cap} \bullet u_{s,t}^{HP}, \text{if } 1 < s \le S \end{cases}, \forall t \in \{1,\ldots,k\} \tag{17}$$

Eq. (18) was used to ensure that the discretization element s was active (i.e. $u_{s,t}^{HP} = 1$) only when the cooling supply related to the previous element in the COP map $\dot{Q}_{s-1,t}^{HP,c}$ was equal to its cooling capacity $\dot{Q}_{s-1}^{HP,c,cap}$.

$$\dot{Q}_{s-1}^{HP,c,cap} - \dot{\boldsymbol{Q}}_{s-1,t}^{HP,c} - \left(1 - \mathbf{u}_{s,t}^{HP}\right) \bullet \sum_{s=1}^{S} \dot{Q}_{s}^{HP,c,cap} \leq 0, \forall s \in \{2, \ldots, S\}, \forall t \in \{1, \ldots, k\} \quad (18)$$

References

[1] IEA. "World energy outlook 2023," Paris, France [Online]. Available: https://www.iea.org/reports/world-energy-outlook-2023; 2023.
[2] IEA. Tracking clean energy progress 2023, Paris, France [Online]. Available: https://www.iea.org/reports/tracking-clean-energy-progress-2023; 2023.
[3] de Boer R, Marina A, Zühlsdorf B, Arpagaus C, Bantle M, Wilk V, et al. Strengthening industrial heat pump innovation: decarbonizing industrial heat. Whitepaper 2020:32. Accessed: Jan. 09, 2024. [Online]. Available: https://orbit.dtu.dk/en/publications/strengthening-industrial-heat-pump-innovation-decarbonizing-indus.
[4] European Environment Agency. Decarbonising heating and cooling — a climate imperative. 2023. https://doi.org/10.2800/515288.
[5] Schlosser F, Jesper M, Vogelsang J, Walmsley TG, Arpagaus C, Hesselbach J. Large-scale heat pumps: applications, performance, economic feasibility and industrial integration. Renew. Sust. Energ. Rev. Nov. 2020;133:110219. https://doi.org/10.1016/j.rser.2020.110219.
[6] Huchtemann K, Müller D. Evaluation of a field test with retrofit heat pumps. Build. Environ. 2012;53:100–6. https://doi.org/10.1016/J.BUILDENV.2012.01.013.
[7] IEA. "The future of heat pumps," Paris, France [Online]. Available: https://www.iea.org/reports/the-future-of-heat-pumps; 2022.
[8] Aguilera JJ, Meesenburg W, Ommen T, Markussen WB, Poulsen JL, Zühlsdorf B, et al. A review of common faults in large-scale heat pumps. Renew. Sust. Energ. Rev. 2022;168:112826. https://doi.org/10.1016/J.RSER.2022.112826.
[9] Pogiatzis T, Ishiyama EM, Paterson WR, Vassiliadis VS, Wilson DI. Identifying optimal cleaning cycles for heat exchangers subject to fouling and ageing. Appl. Energy Jan. 2012;89(1):60–6. https://doi.org/10.1016/J.APENERGY.2011.01.063.
[10] Cuisinier E, Bourasseau C, Ruby A, Lemaire P, Penz B. Techno-economic planning of local energy systems through optimization models: a survey of current methods. Int. J. Energy Res. 2021;45(4):4888–931. https://doi.org/10.1002/er.6208.
[11] Lindberg KB, Doorman G, Fischer D, Korpås M, Ånestad A, Sartori I. Methodology for optimal energy system design of zero energy buildings using mixed-integer linear programming. Energ Buildings Sep.2016;127:194–205. https://doi.org/10.1016/J.ENBUILD.2016.05.039.
[12] Bojić M, Dragičević S. MILP optimization of energy supply by using a boiler, a condensing turbine and a heat pump. Energy Convers. Manag. Mar.2002;43(4):591–608. https://doi.org/10.1016/S0196-8904(01)00028-0.
[13] Fink J, van Leeuwen RP, Hurink JL, Smit GJM. Linear programming control of a group of heat pumps. Energy Sustain. Soc. Dec.2015;5(1):1–10. https://doi.org/10.1186/S13705-015-0061-9/FIGURES/4.
[14] Beck T, Kondziella H, Huard G, Bruckner T. Optimal operation, configuration and sizing of generation and storage technologies for residential heat pump systems in the spotlight of self-consumption of photovoltaic electricity. Appl. Energy Feb. 2017;188:604–19. https://doi.org/10.1016/J.APENERGY.2016.12.041.
[15] Verhelst C, Logist F, Van Impe J, Helsen L. Study of the optimal control problem formulation for modulating air-to-water heat pumps connected to a residential floor heating system. Energ Buildings Feb. 2012;45:43–53. https://doi.org/10.1016/J.ENBUILD.2011.10.015.
[16] Ommen T, Jensen J, Meesenburg W. Generalized COP estimation of heat pump processes for operation off the design point of equipment. In: Proceedings of the 25th IIR International Congress of Refrigeration; 2019. p. 8. https://doi.org/10.18462/iir.icr.2019.0648.
[17] Jensen JK, Ommen T, Reinholdt L, Markussen WB, Elmegaard B. Heat pump COP, part 2: Generalized COP estimation of heat pump processes. In: Proceedings of the 13th IIR-Gustav Lorentzen Conference on Natural Refrigerants; 2018. p. 1136–45. https://doi.org/10.18462/iir.gl.2018.1386.
[18] Pieper H, Krupenski I, Brix Markussen W, Ommen T, Siirde A, Volkova A. Method of linear approximation of COP for heat pumps and chillers based on thermodynamic modelling and off-design operation. Energy 2021;230:120743. https://doi.org/10.1016/j.energy.2021.120743.
[19] Wirtz M, Neumaier L, Remmen P, Müller D. Temperature control in 5th generation district heating and cooling networks: an MILP-based operation optimization. Appl. Energy Apr. 2021;288:116608. https://doi.org/10.1016/J.APENERGY.2021.116608.
[20] Krützfeldt H, Vering C, Mehrfeld P, Müller D. MILP design optimization of heat pump systems in German residential buildings. Energ Buildings Oct.2021;249:111204. https://doi.org/10.1016/J.ENBUILD.2021.111204.
[21] Maier L, Schönegge M, Henn S, Hering D, Müller D. Assessing mixed-integer-based heat pump modeling approaches for model predictive control applications in buildings. Appl. Energy Nov. 2022;326:119894. https://doi.org/10.1016/J.APENERGY.2022.119894.
[22] Lee Z, Gupta K, Kircher KJ, Zhang KM. Mixed-integer model predictive control of variable-speed heat pumps. Energ Buildings Sep. 2019;198:75–83. https://doi.org/10.1016/j.enbuild.2019.05.060.
[23] Gomes ILR, Ruano MG, Ruano AE. MILP-based model predictive control for home energy management systems: a real case study in Algarve, Portugal. Energ Buildings Feb. 2023;281:112774. https://doi.org/10.1016/J.ENBUILD.2023.112774.
[24] D'Ettorre F, Conti P, Schito E, Testi D. Model predictive control of a hybrid heat pump system and impact of the prediction horizon on cost-saving potential and optimal storage capacity. Appl. Therm. Eng. Feb. 2019;148:524–35. https://doi.org/10.1016/J.APPLTHERMALENG.2018.11.063.
[25] Efkarpidis NA, Vomva SA, Christoforidis GC, Papagiannis GK. Optimal day-to-day scheduling of multiple energy assets in residential buildings equipped with variable-speed heat pumps. Appl. Energy Apr. 2022;312:118702. https://doi.org/10.1016/J.APENERGY.2022.118702.
[26] Moser A, Muschick D, Gölles M, Nageler P, Schranzhofer H, Mach T, et al. A MILP-based modular energy management system for urban multi-energy systems: performance and sensitivity analysis. Appl. Energy Mar. 2020;261:114342. https://doi.org/10.1016/J.APENERGY.2019.114342.
[27] You Z, Lumpp SD, Doepfert M, Tzscheutschler P, Goebel C. Leveraging flexibility of residential heat pumps through local energy markets. Appl. Energy Feb. 2024;355:122269. https://doi.org/10.1016/J.APENERGY.2023.122269.
[28] Liang X, Chen K, Chen S, Zhu X, Jin X, Du Z. IoT-based intelligent energy management system for optimal planning of HVAC devices in net-zero emissions PV-battery building considering demand compliance. Energy Convers. Manag. 2023;292:117369. https://doi.org/10.1016/j.enconman.2023.117369.
[29] Bünning F, Warrington J, Heer P, Smith RS, Lygeros J. Robust MPC with data-driven demand forecasting for frequency regulation with heat pumps. Control. Eng. Pract. 2022;122:105101. https://doi.org/10.1016/j.conengprac.2022.105101.
[30] Nielsen MG, Morales JM, Zugno M, Pedersen TE, Madsen H. Economic valuation of heat pumps and electric boilers in the Danish energy system. Appl. Energy Apr. 2016;167:189–200. https://doi.org/10.1016/J.APENERGY.2015.08.115.
[31] Klingebiel J, Salamon M, Bogdanov P, Venzik V, Vering C, Müller D. Towards maximum efficiency in heat pump operation: self-optimizing defrost initiation control using deep reinforcement learning. Energ Buildings Jul. 2023:113397. https://doi.org/10.1016/J.ENBUILD.2023.113397.
[32] Chen WD, Hasanien HM, Chua KJ. Towards a digital twin approach – experimental analysis and energy optimization of a multi-bed adsorption system. Energy Convers. Manag. Nov. 2022;271:116346. https://doi.org/10.1016/J.ENCONMAN.2022.116346.
[33] Zhang K, Wu Q, Li H, Zhang R, Li J, Jiang F, et al. Intelligent optimal control strategy of heat pump system based on digital twins. J. Phys. Conf. Ser. 2023;2452(1):12029. https://doi.org/10.1088/1742-6596/2452/1/012029.
[34] Aguilera JJ, Meesenburg W, Markussen WB, Poulsen JL, Zühlsdorf B, Elmegaard B. Adaptive model-based monitoring of large-scale heat pump prone to evaporator fouling. In: Proceedings of the 26th International Congress of Refrigeration; 2023. p. 12.
[35] Gjengedal S, Stenvik LA, Ramstad RK, Ulfsnes JI, Hilmo BO, Frengstad BS. Online remote-controlled and cost-effective fouling and clogging surveillance of a groundwater heat pump system a case study from Lena terrace in Melhus, Norway. Bull. Eng. Geol. Environ. 2021;80:1063–72. https://doi.org/10.1007/s10064-020-01963-z.
[36] Modelica-Association. Modelica and the Modelica Standard Library. 2021.
[37] Microsoft Corporation. Azure API Management [Online]. Available, https://azure.microsoft.com/; 2023 [accesed 7 December 2023].
[38] Church P, Mueller H, Ryan C, Gogouvitis SV, Goscinski A, Haitof H, et al. SCADA Systems in the Cloud. In: Zomaya AY, Sakr S, editors. Handbook of big data technologies. Cham: Springer International Publishing; 2017. p. 691–718. https://doi.org/10.1007/978-3-319-49340-4_20.
[39] Danish Meteorological Institute. DMI Open Data Portal. Version 1.30.18 [Online]. Available, https://dmiapi.govcloud.dk/; 2023 [accesed 7 December 2023].
[40] Pecinovsky J, Boerman F. Entsoe-py. Version 1.2.0 [Online]. Available, https://github.com/EnergieID/entsoe-py/; 2023 [accesed 7 December 2023].
[41] Madsen H. Time series analysis. CRC Press; 2007.
[42] Seabold S, Perktold J. Statsmodels: Econometric and statistical modeling with python. Version 0.15.0. In: 9th Python in Science Conference. Austin, Texas; 2010. p. 92–6 [Online]. Available, https://www.statsmodels.org/ [accesed 7 December 2023].
[43] Dassault Systèmes. Dymola: Dynamic Modeling Laboratory. Version 2021x [Online]. Available, https://www.3ds.com/products/catia/dymola/; 2023 [accesed 7 December 2023].
[44] TLK-Thermo GmbH. TIL Suite and TILMedia for Modelica. Version 3.12.0 [Online]. Available, https://www.tlk-thermo.com/; 2023 [accesed 7 December 2023].
[45] Dassault Systèmes. FMPy. Version 0.3.14 [Online]. Available, https://fmpy.readthedocs.io/; 2023 [accesed 7 December 2023].
[46] Wüllhorst F, Storek T, Mehrfeld P, Müller D. AixCaliBuHA: automated calibration of building and HVAC systems. J. Open Source Softw 2022;7(72):3861. https://doi.org/10.21105/joss.03861.
[47] Virtanen P, Gommers R, Oliphant TE, Haberland M, Reddy T, Cournapeau D, et al. SciPy 1.8.0: fundamental algorithms for scientific computing in Python. Nat. Methods 2020;17(3):261–72. https://doi.org/10.1038/s41592-019-0686-2.
[48] Gurobi Optimization LL. Gurobi: Gurobi optimizer. Version 11.0.0 [Online]. Available, https://www.gurobi.com/; 2023 [accesed 8 December 2023].

[49] Moretti L, Manzolini G, Martelli E. MILP and MINLP models for the optimal scheduling of multi-energy systems accounting for delivery temperature of units, topology and non-isothermal mixing. Appl. Therm. Eng. Feb. 2021;184:116161. https://doi.org/10.1016/J.APPLTHERMALENG.2020.116161.

[50] Chiam Z, Easwaran A, Mouquet D, Fazlollahi S, Millás JV. A hierarchical framework for holistic optimization of the operations of district cooling systems. Appl. Energy Apr. 2019;239:23–40. https://doi.org/10.1016/J.APENERGY.2019.01.134.

[51] Muschick D, Zlabinger S, Moser A, Lichtenegger K, Gölles M. A multi-layer model of stratified thermal storage for MILP-based energy management systems. Appl. Energy May 2022;314:118890. https://doi.org/10.1016/J.APENERGY.2022.118890.

[52] Danish Meteorological Institute. "Be aware of the uncertainty in the weather forecast (in Danish)," Copenhagen, Denmark [Online]. Available, https://www.dmi.dk/nyheder/2020/bliv-klog-paa-usikkerheden-i-vejrudsigten; 2020 [accesed 5 January 2024].

[53] Powell KM, Sriprasad A, Cole WJ, Edgar TF. Heating, cooling, and electrical load forecasting for a large-scale district energy system. Energy Sep. 2014;74:877–85. https://doi.org/10.1016/J.ENERGY.2014.07.064. no. C.

[54] Sarwar R, Cho H, Cox SJ, Mago PJ, Luck R. Field validation study of a time and temperature indexed autoregressive with exogenous (ARX) model for building thermal load prediction. Energy Jan. 2017;119:483–96. https://doi.org/10.1016/J.ENERGY.2016.12.083.

[55] Kurek T, Bielecki A, Świrski K, Wojdan K, Guzek M, Białek J, et al. Heat demand forecasting algorithm for a Warsaw district heating network. Energy Feb. 2021;217:119347. https://doi.org/10.1016/J.ENERGY.2020.119347.

[56] Meesenburg W, Aguilera JJ, Kofler R, Markussen WB, Elmegaard B. Prediction of fouling in sewage water heat pump for predictive maintenance. In: Proceedings of ECOS 2022: 35th international conference on efficiency, Cost, Optimization, Simulation and Environmental Impact of Energy Systems; 2022. p. 12.